

## Article

# Polymer-Metal Adhesion of Single-Lap Joints Using Fused Filament Fabrication Process: Aluminium with Carbon Fiber Reinforced Polyamide

Guilherme Martins <sup>1</sup>, Carlos M. S. Vicente <sup>1,2,\*</sup> and Marco Leite <sup>1,2</sup><sup>1</sup> IST, Instituto Superior Técnico, Universidade de Lisboa, Av. Rovisco Pais, 1049-001 Lisbon, Portugal<sup>2</sup> IDMEC, Instituto Superior Técnico, Universidade de Lisboa, Av. Rovisco Pais, 1049-001 Lisbon, Portugal

\* Correspondence: carlos.vicente@tecnico.ulisboa.pt

**Abstract:** Additive manufacturing (AM) is often used for prototyping; however, in recent years, there have been several final product applications, namely the development of polymer-metal hybrid (PMH) components that have emerged. In this paper, the objective is to characterize the adhesion of single-lap joints between two different materials: aluminium and a polymer-based material manufactured by fused filament fabrication (FFF). Single-lap joints were fabricated using an aluminium substrate with different surface treatments: sandpaper polishing (SP) and grit blasting (GB). Three filaments for FFF were tested: acrylonitrile butadiene styrene (ABS), polyamide (PA), and polyamide reinforced with short carbon fibers (PA + CF). To characterize the behaviour of these single-lap joints, mechanical tension loading tests were performed. The analysis of the fractured surface of the joints aimed to correlate the adhesion performance of each joint with the occurred failure mode. The obtained results show the impact of surface roughness ( $0.16 < Ra < 1.65 \mu\text{m}$ ) on the mechanical properties of the PMH joint. The ultimate lap shear strength (ULSS) of PMH single-lap joints produced by FFF ( $1 < \text{ULSS} < 6.6 \text{ MPa}$ ) agree with the reported values in the literature and increases for substrates with a higher surface roughness, remelting of the primer (PA and PA + CF), and higher stiffness of the polymer-based adherent.



**Citation:** Martins, G.; Vicente, C.M.S.; Leite, M. Polymer-Metal Adhesion of Single-Lap Joints Using Fused Filament Fabrication Process: Aluminium with Carbon Fiber Reinforced Polyamide. *Appl. Sci.* **2023**, *13*, 4429. <https://doi.org/10.3390/app13074429>

Academic Editors: Alberto Corigliano and Richard (Chunhui) Yang

Received: 13 January 2023  
Revised: 23 March 2023  
Accepted: 28 March 2023  
Published: 30 March 2023



**Copyright:** © 2023 by the authors. Licensee MDPI, Basel, Switzerland. This article is an open access article distributed under the terms and conditions of the Creative Commons Attribution (CC BY) license (<https://creativecommons.org/licenses/by/4.0/>).

**Keywords:** fused filament fabrication; polymer-metal adhesion; single-lap joints; carbon fiber

## 1. Introduction

Current global policies in place plan to decrease greenhouse gas emissions, creating a path for the world to become climate neutral by 2050 [1,2]. The European Union clearly sets a common goal for every enterprise, where ecology and digital transformation come together towards an enhanced portfolio of leading European sustainability companies [3]. Joining dissimilar materials can be highly demanding [4], but has the potential to increase a product's functionality and manufacturing efficiency, which is in alignment with the EU's sustainability objectives. Joining dissimilar materials spans multiple approaches and materials, which can increase its complexity in relation to other manufacturing techniques [5]. Examples of these applications can be found in the automotive [6,7], aeronautics [8–10], textile [11], and tooling sectors [12], among many others [13].

The ever-increasing demand for sustainable and complex components opens a window of opportunity for additive manufacturing (AM) techniques that, after decades of improvement, began to fabricate end-use products rather than simple parts and prototypes [14]. Because AM is a tool-less technology it has flexibility to generate complex parts without increasing costs, and is an interesting option for many companies worldwide to adopt and fabricate products with it [15,16]. One possible application is to use AM to fabricate parts and specimens with dissimilar materials due to the potential to create optimal, lightweight, and high-performance components [5]. Regardless of the interest in dissimilar materials using AM techniques, adopting the combining of aluminium and

polymers using AM is far from widespread. There are several challenges to overcome, but the potential for the automotive, power production, aerospace, medical, and many other sectors exists [5]. Challenges arise with materials of different chemical, mechanical, thermal, or electrical properties, or when those produced by different processes are to be joined together, namely regarding the structural integrity of the joints [9]. Comparing with others' materials, polymer/metal components are the best in terms of ease of manufacture and increased weight-to-strength ratio [17]. The ability to fabricate such parts, added to industry's significant demand for them, provides a strong advantage to some AM techniques [18,19].

Among the available AM techniques [20], fused filament fabrication (FFF) is now perceived as one major AM technology platform to produce polymer/metal multi-material components [21–23]. The FFF is an AM technique that starts with filament material being guided to the extruder, where torque and a pinch system is used to feed and retract precise amounts of it. A heater block then heats the filament to a controllable temperature that is well above the glass transition temperature of amorphous polymers or the melting point of semi-crystalline ones [24,25], and is forced out of the heated nozzle. The extruded material is laid down on the model through the correct positioning of the print head and/or the build plate, placing the material where it is needed [26,27]. The value of FFF techniques for rapid prototyping or end-user products is undeniable [28]. However, the process is highly dependent on the optimization of numerous parameters to achieve parts with a high-quality surface finish [29–32], dimensional accuracy [32,33], and mechanical performance [32,34–37].

Adhesive joining is the most appropriate technique for bonding metallic and non-metallic structures where the strength-to-weight ratio must be maximized [38]. This technique utilizes polymeric substrates to join a large variety of material combinations. The adhesive joining between polymer-based materials and metals often involves the application of heat and pressure [39,40].

The literature identifies six main mechanisms of adhesion [41,42]: absorption [43], electrostatic attraction [44,45], chemical bonding [46], mechanical interlocking [47–49], diffusion [50], and a weak boundary layer [51]. A proper compatibility of the interface between both substrates desired is of extreme importance to form the adhesive joint. A mixture of adhesion mechanisms is usually responsible for a given system [52], since a definitive conclusion on which mechanisms best suit adhesive bonding is still lacking.

Surface treatments are currently being used to improve this adhesion. An increase in the friction coefficient correlates with an increment in the surface roughness of the material [53,54]. Furthermore, an increase in wettability when combining the incorporation of polar functional groups to a polymer joined with a silicon coated steel positively influences the adhesion strength [54,55]. The grit-blasting technique is believed to be the ideal surface treatment for metallic media [43,56,57]. Despite these surface treatments, some substrates may still provide only negligible adhesion. At this point, primers or adhesive promoters may come to aid with further improvements of the joining strength [58,59]. The adhesion strength evaluation can be performed by mechanical tests (tensile, shear and peel tests) [60], or by nondestructive tests [61], which also permit the assessment of damage of the joints [62].

Previous works explored the potential of ABS and polyamides (PA) in terms of being successfully coated with metals, evidencing the potential of using these polymers when joining dissimilar materials [63–66]. The ABS arises as an ideal choice for engineering applications, as it possesses high toughness, mechanical strength, good thermal stability, and cheapness, to name a few advantages of it [36,67–70]. On the other hand, reinforced PA can also be classified as a high-performance engineering material, since the presence of fillers within a PA matrix enhances its mechanical properties and decreases the influence of humidity [71]. Some constraints must be pointed out with regard to using these polymers in FFF applications. The most inconvenient one for the conduction of this experiment was the warping effect (a non-wanted distortion on the surfaces of a part), which is already

extensively described in numerous papers and is frequent when printing with PA and ABS filaments [72,73].

In recent years, several works reported the use of AM to produce parts with polymer-metal hybrid materials (PMHM), demonstrating the timeliness and growing interest in this technology. The first study of this technology using AM was undertaken by Cham et al. [74], where the design and manufacturing of products with embedding components through a layered process termed Shaped Deposition Manufacturing was addressed. This work presents a combination of process planning algorithms and manufacturing methods for the design of parts with PMHM, and provides an insight into the multiple applications of these components in industries such as automotive and electrical systems [74]. In addition to aspects related to product design and process planning, it is crucial to study the mechanical properties of parts produced with PMHM in order to successfully implement this technology. The mechanical properties of PMHM structures comprised of a photoresin and an amorphous layer metal (NiB) obtained by 3D printing and electroless deposition, respectively, were studied in the work of Mieszala et al. [75]. The authors focused on the deformation mechanisms and energy absorption capability of cellular structures produced with these PMHM, and found that chemical bonding is essential in promoting a good adhesion between the polymer and metal in these microstructures. The mechanical properties of PMHM joints obtained by a combination of laser powder bed fusion (LPBF) and FFF processes were studied in the work of Chueh et al. [55]. The proposed fabrication method starts with the production of metal (stainless steel) interlocking structures by LPBF, followed by the deposition by FFF of the melted polymer (PLA or PET) on the top of the metallic substrate. During the FFF process, the substrate is heated to decrease the polymer's viscosity and facilitate its flow into those metal interlocking structures. In the final step of the process, the melted plastic material is compressed and the laser is scanned, boosting the inter-molecular adhesion between the metal and polymer. The use of the FFF process is of great interest given its widespread use in commercial 3D printers. However, the application of FFF technology with the use of PMHM still requires further study. In 2017, Fanferot et al. [21] demonstrated the deposition of PMHM with the FFF process using polymer-metal hybrid filaments, and PLA reinforced with bronze and iron. The mechanical properties of the parts were studied, and the authors concluded that although the tensile strength of parts produced with hybrid materials were similar to the ones of PLA, the interfacial adhesion of PMHM was reduced when compared with the PLA. The FFF process was also employed to fabricate PMHM joints between aluminium and ABS [22,23], or between aluminium and alternate layers of polyamides (PA) and continuous carbon fiber (CF) reinforced PA [22], in a process referred to as the AddJoining technique. The authors observed that the mechanical behavior of the AddJoining parts is comparable to the joints produced with state-of-the-art adhesive bonding.

Due to the popularity of FFF equipment and the need to understand the mechanisms of joining dissimilar materials, in this work the feasibility of adhesion between aluminium and three polymer-based materials: ABS, PA and PA reinforced with short CF, was studied. Single-lap joints of aluminium substrate with polymer-based adherents were produced by FFF using a customized printing bed. The effect of surface roughness and the presence of fibres on the adhesion strength between each pair of materials was also studied. The experimental work includes standard tensile tests, optical profilometry measurements, and morphological observations using scanning electron microscopy (SEM). The analysis of the fractured surfaces and failure modes of the single-lap joints was also performed. To the best of our knowledge, this is the first time that the adhesion of single-lap joints of aluminum-PA and aluminum-(PA-CF) produced by FFF was reported, and it correlated with the aluminum surface roughness and the failure modes of the joints.

## 2. Materials and Methods

### 2.1. Materials

As previously mentioned, single-lap joints with two different adherents were fabricated. The single-lap joints consisted of a metallic substrate and a polymer based top layer. The geometry of the specimens, as seen in Figure 1, was derived from ASTM D3163-01 standard [76]. There is an interfacing section between the two materials that is 12 mm in length and 26 mm in width.

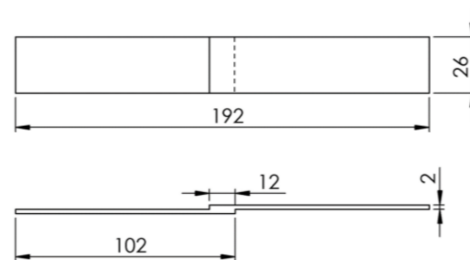


**Figure 1.** Specimen geometry used for single-lap joints.

The substrate, with a thickness of 2 mm, is made of commercial aluminium with 265 MPa of ultimate tensile stress (UTS) and 235 MPa of yield stress. The Young's modulus ( $E$ ) of 78.8 GPa and 3.92% elongation at break were registered. These values were obtained from an experimental test using an INSTRON 3369 universal testing machine with a 50 kN load cell and a crosshead speed of 1.0 mm/min. Three specimens were machined and tested following the ASTM E8/E8M—13a standard [77].

For the top polymer-based adherent, ABS, PA, and PA reinforced with CF (PA + CF), 1.75 mm filaments were used. The ABS filament was acquired from Makerbot. The general properties of ABS plastic (UTS = 27.6–55.2 MPa and  $E$  = 1.19–2.90 GPa) were obtained in the literature [67–69]. The PA acquired from Markforged was used for the second set of specimens. General properties for this PA (UTS = 36 MPa and  $E$  = 1.70 GPa) can be found in the literature [78]. PA + CF was acquired from Fillamentum, and is characterized by the following properties: UTS = 54.5 MPa and  $E$  = 0.5 GPa [79].

### 2.2. Fabrication of Specimens

The printer used in this work was a Raise3D Pro2. Due to the geometry of the specimens, the 3D printer bed was adapted to level the aluminium substrate with the printer bed. The original build plate from the Raise system was replaced by a customized one. This customized build plate was fabricated with the same aluminium sheet employed for obtaining the substrates of the single-lap joints, with a slot to insert the base substrate, as shown in Figure 2. Note that any other material can be used as long as the slot has the same thickness of the specimen and allows for the adhesion of the deposited polymer.

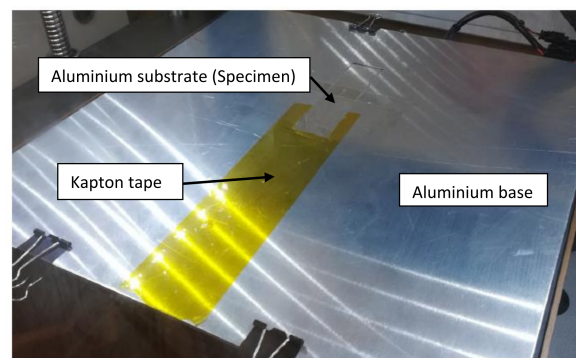


**Figure 2.** 3D printer customized base.

The first step for the fabrication of specimens was to validate the printing parameters for each filament. A standard profile for ABS was used. However, to ensure that the parts did not warp, which is a common issue with ABS 3D printing [80], the build plate temperature and the application of the brim loop lines were studied in greater detail. The remaining 3D printing parameters were fixed for each filament, as specified in the manufacturer's printing guides and based on previous work with same materials [23,79], as shown in Table 1. A build plate temperature of 110 °C and Kapton tape was used. The Kapton tape assured a proper adhesion of the ABS during printing, and made for easier removal after its completion. For PA, the build plate temperature was also set to 110 °C, but for this material blue masking tape was employed, as it was noticeably better at preventing the warping of the specimen. In this case, it was necessary to use 25 brim lines to secure the specimen. For PA reinforced with CF, the building plate temperature was also set to 110 °C, with blue masking tape and 45 brim lines.

**Table 1.** 3D printed parameters for each filament.

Filament	Printing Temperature (°C)	Infill Percentage	Deposition Speed (mm/s)	Layer Thickness (mm)	Raster Angle (°)	Number of Contours
ABS	280	100	50	0.1	±45	12
PA	270	100	45	0.1	±45	12
PA + CF	260	100	30	0.1	±45	12

Due to the need to improve the adhesion with blue tape or Kapton tape, between the aluminium base and the 3D printed material (in the region outside the joint) it was clear that the surface where the joint was formed must be prepared in order to improve the adhesion between the aluminium substrate and the 3D printed material.

### 2.3. Surface Preparation of the Joints

The adhesion between the aluminium and the 3D printed material in the joint region was improved by employing two consecutive strategies. The first strategy was to increase the surface roughness of the aluminium substrate through sandpaper polishing (SP) or grit blasting (GB) techniques, followed by the second strategy, which consisted of the application of a primer on top of the aluminium substrate prior to the 3D printing process.

The SP process was applied using sandpaper with particles with an average diameter of 125 µm, and the polishing direction was varied alternately between 0 and 180° in order to create a uniform pattern. The GB technique was performed on a RP-TOOLS 350 L machine with brown corundum particles (Al<sub>2</sub>O<sub>3</sub>) with an average granulate size of 256 µm and a pressure of 6 bar for a period of 20 s. During the GB process, each substrate was placed at an angle of 45° relative to the blasting nozzle, with a working distance of 200 mm. The blasting direction varied alternately between 0, 90, +45 and −45° in order to create a uniform blasting pattern [81]. The specimens were cleaned with isopropyl alcohol and compressed air after each of these mechanical abrasion processes.

For aluminium-ABS joints, an ABS primer was manually spread with a paintbrush following the procedure of Falck et al. [22,23], as shown in Figure 3a,b. The ABS primer was obtained by the dissolution of small portions of the ABS filament (5 mm length) in acetone for 24 h, giving rise to a 25 wt.% ABS solution. On the aluminium-PA and aluminium-PA + CF's joints, the application of the primer was done by FFF, using PA and PA + CF, respectively, and is shown in Figure 3c. For the aluminium-PA and aluminium-PA + CF's joints, the primer was remelted on a hotplate at 270 °C for 1 min in order to better infiltrate the cavities on the surface of the aluminium substrate, as shown in Figure 3d. Several FFF depositions were performed (aiming to produce single-lap joints) on the surfaces of the previously prepared aluminium substrates using SP and abrasion with the GB technique and the application of the primer. Table 2 shows the successful and unsuccessful results of

the FFF depositions that aimed to make adhesive joints between the aluminium and the 3D printed materials.

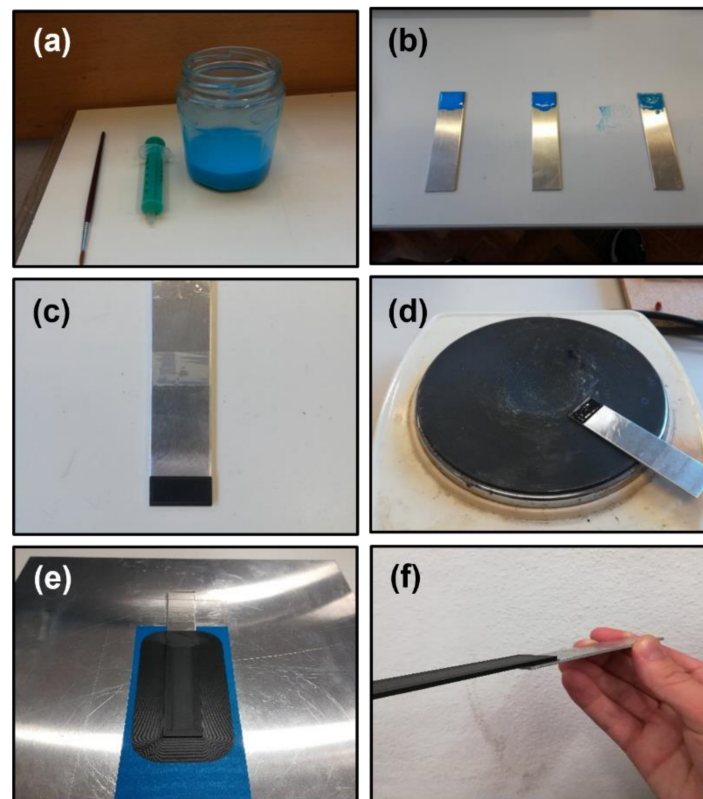


**Figure 3.** (a) ABS primer's application tools; (b) three examples of base material with primer applied; (c) PA + CF specimen after the application of the primer by FFF; (d) remelting of the PA + CF primer on top of a hot plate; (e) aluminium–PA + CF single-lap joint resting time after 3D printing; and (f) aluminium–PA + CF single-lap joint after removal from the printer.

**Table 2.** Single-lap joints results: filaments, surface treatments and primer.

Filament	Surface Treatment	Primer	Single-Lap Joint
ABS	SP	No	Fail
		Yes	Fail
	GB	No	Fail
		Yes	Success
PA	SP	No	Fail
		Yes	Success
	GB	No	Fail
		Yes	Success
PA + CF	SP	No	Fail
		Yes	Success
	GB	No	Fail
		Yes	Success

It should be noted that only samples where a primer was applied gave rise to successful single-lap joints with the adhesion between the aluminium substrate and the polymer-based adherent. For PA and PA + CF, both SP and GB techniques had satisfactory results, as shown in Figure 3e,f, while for ABS the GB technique was the only successful one.

#### 2.4. Optical Profilometry

In order to compare the different surface treatments and their effects on the lap-shear strength of the PMHM joints, an optical profilometry measurement was done on the top surface of the base material. The profilometry measurements based on the white light interferometry method were performed on the profilometer Profilm 3D with a 20× objective. The scanned surface area was  $1.0 \times 0.85 \text{ mm}^2$ . The raw data was acquired using envelope peak analysis. The raw data files were exported and post-processed with the software Profilm Online [82]. The average surface roughness (Ra) and the maximum surface roughness (Rz) of the base material's top surface were determined by considering the entire scanned area for both the abraded and non-abraded samples. For each experimental condition, three areas representative of the aluminium surface were considered.

#### 2.5. Scanning Electron Microscopy

A scanning electron microscope (SEM) analysis was conducted to characterize the interface and morphology of the PMHM joints. A slice of the PMHM joints was cut and fixed in a resin structure. After it had cured, the joint surface was polished with traditional sandpapers and silicon carbide sandpapers for final finishing. The SEM images were obtained with a field emission type microscope (JEOL 7001F FEG-SEM) operating at 5.0 kV in secondary electron emission mode. The surface of specimens was fixed on the SEM sample holder with a conductive adhesive. The thicknesses of the primers present in the joints were estimated by a graphical analysis of the SEM images.

#### 2.6. Single-Lap Joints—Mechanical Tests

The strength of PMHM single-lap joints were quantified by a single-lap tension loading test. The tension loading tests were performed in an INSTRON 3369 with a 50 kN load cell and a crosshead speed equal to 1.27 mm/min. The tension loading tests followed the procedure from the ASTM D3163 standard test [76]. Given the design of single-lap joints (Figure 1), it was important to prevent the characteristic bending effect of single-lap joints subjected to tension loading. Therefore, two pieces of the same aluminium sheet as the substrate material were placed one each on the inner sides of the substrate and polymer strip before placing the specimens into the grips of the testing machine. Thus, the line of action of the force applied during the tests was aligned with both surfaces of the adherends. The following properties were extracted from the mechanical tests: the ultimate lap shear strength (ULSS) and the elastic modulus of the lap-joint (E).

### 3. Results and Discussion

#### 3.1. Surface Roughness of the Substrate

The surface of the aluminium was analysed with the goal of determining the surface roughness of our substrate base material before the formation of the PMHM joint. The raw data of the surface roughness profiles obtained for the different surface conditions are displayed on Figure 4.

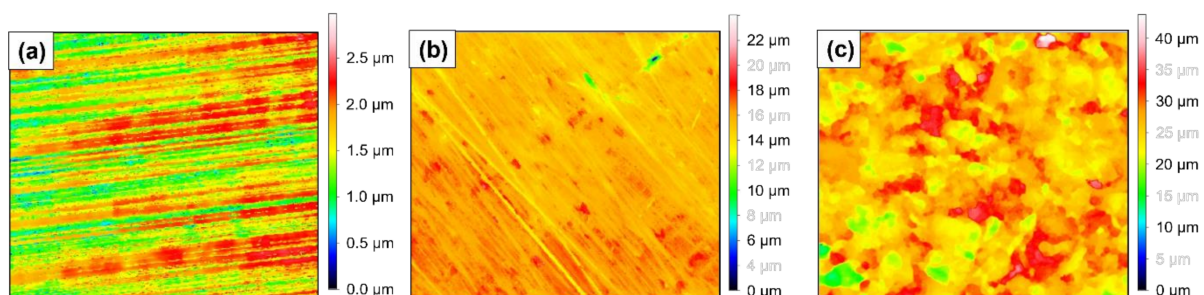


**Figure 4.** Optical profilometry's 3D profiles of the aluminium: (a) without any surface treatment, (b) after being polished by SP, and (c) after the GB process.

The raw data presented in Figure 4 allow us to make a comparison of surfaces exposed to different surface treatments. The optical profilometry results revealed a higher surface roughness in the SP and GB surfaces when compared with the aluminium surface without any surface treatment. The SP and GB techniques lead to the homogenisation of roughness and the increased roughness of the aluminium surface. The small sharp peaks present on the surface of untreated aluminium (Figure 4a) were converted into a more uniform roughness distribution for both SP and GB surfaces. The higher degree of abrasion was found in the GB surfaces, where the rounded shapes of its valleys, resulting from the impact of the projected particles during the GB process, were noticeable. The respective values of the Ra and Rz obtained are displayed in Table 3.

**Table 3.** Values of surface roughness of aluminium for the non-treated and treated surface conditions.

	Surface Treatment		
	None	SP	GB
Ra [ $\mu\text{m}$ ]	$0.16 \pm 0.04$	$0.32 \pm 0.05$	$1.65 \pm 0.46$
Rz [ $\mu\text{m}$ ]	$0.58 \pm 0.12$	$1.12 \pm 0.22$	$6.20 \pm 1.67$

The surface roughness obtained for the aluminium substrate without any treatment (Ra = 0.16  $\mu\text{m}$  and Rz = 0.58  $\mu\text{m}$ ) is in accordance with the values reported on other studies (Ra = 0.18  $\mu\text{m}$  and Rz = 0.8  $\mu\text{m}$ ) in which the surface roughness of aluminium substrates was estimated, before the formation of PMHM joints [22,23,83]. For the treated surface conditions, the direct comparison of the surface roughness values with previous works becomes more difficult, as these values are dependent on the process parameters. However, it is worthy of note that the values obtained for SP aluminium (Ra = 0.32  $\mu\text{m}$  and Rz = 1.12  $\mu\text{m}$ ) are in the range of the surface roughness values reported by Boutar et al. (Ra = 0.3 to 3  $\mu\text{m}$ ) [84], but well below the range ( $0.7 < \text{Ra} < 3.15 \mu\text{m}$ ) reported in similar works where the SP was applied on the aluminium of single-lap joints [85–87]. The surface roughness values of aluminium after the GB treatment (Ra = 1.65  $\mu\text{m}$  and Rz = 6.20  $\mu\text{m}$ ) are comparable with the values (Ra = 1.9  $\mu\text{m}$ ) reported by Bechtel et al. [83], but well below the values reported by Goushegir et al. (Ra = 5.2  $\mu\text{m}$ ) [85], or by Falck et al. (Rz = 89  $\mu\text{m}$ ) [22,23]. In addition to SP and GB surface treatments, there are other methods to increase the surface roughness of the aluminium used in PMHM single-lap joints. Some authors report the use of techniques such as shot peening (Ra = 2 and 6  $\mu\text{m}$ ) [88], chemical etching (Ra = 1.7–1.92  $\mu\text{m}$ ) [86,89], or anodization (Ra = 2.13–4.77  $\mu\text{m}$ ) [89].

### 3.2. Interfaces and Morphology

The SEM's analysis of the cross sections of the PMHM joints revealed the characteristic layered structure of 3D printed polymer-based materials where the air gaps between printed rasters are visible, as shown in Figure 5. The SEM results allowed for the estimation of the primer thicknesses present in the PMHM joints. The primer for the aluminium-ABS single lap-joint was applied manually and, therefore, was of an unknown thickness, while for aluminium-PA and aluminium-PA + CF single-lap joints, the primers were manufactured by FFF, and its thickness was set to be 0.1 mm in the software of the 3D printer. The SEM results indicated a thickness of 0.125 mm for the aluminium-ABS single lap joints, and validated the programmed 0.1 mm primer's thickness for the PMHM joints produced with PA and PA + CF. The values obtained for the thickness of the primer in the joints agrees with those obtained by Objois et al. and their findings with regard to the influence of the thickness of the adhesive, on the extent of microcrack initiation, fracture propagation and, consequently, breaking stress [59]. In this work, the authors conclude that the optimal value of the adhesive thickness in order to achieve the maximum mechanical strength of the joint (a steel-steel single-lap joint glued with epoxy resin) was close to 0.1 mm.

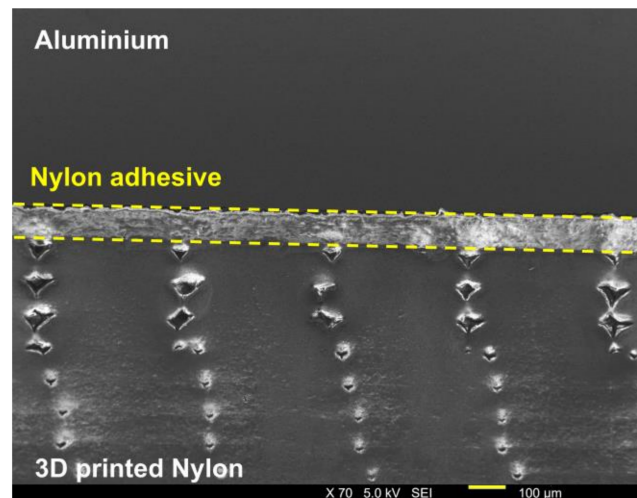


**Figure 5.** SEM image of a cross section of a single-lap aluminium-PA + CF joint.

Another SEM's analysis was conducted on the single-lap joints produced with PA + CF, with the objective of evaluating the possible infiltration of fibers on the surface of aluminium. However, the results from this analysis were inconclusive, as it was difficult to obtain a magnified SEM image of the aluminium-PA + CF interface.

### 3.3. Mechanical Properties

The mechanical properties ULSS and E of the studied single-lap joints are displayed in Figure 6, and indicate the average values obtained from the experimental data. The raw data for all the tested specimens can be found in Supplementary Materials.

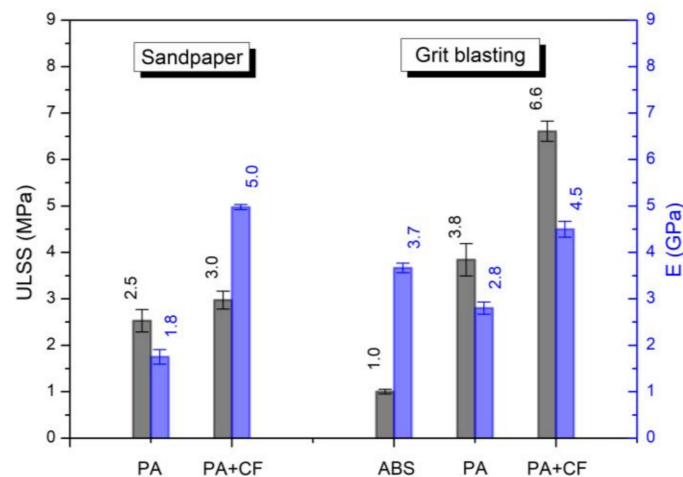


**Figure 6.** Mechanical properties (ULSS and E) of PMHM joints.

From the data presented in Figure 6, we can observe an increase in ULSS when we consider the single-lap joints produced in aluminium treated with the GB technique. This increase in mechanical properties is probably linked to an increase in adhesion (by the mechanical interlocking effect) caused by a greater surface roughness of the aluminium substrate [54,88]. The same increase in the mechanical properties of single-lap joints (when higher values for the surface roughness are considered) was verified for aluminium-aluminium single-lap joints glued with a polyurethane (PU) adhesive [84], aluminium-ABS single-lap joints [23], aluminium-PA single-lap joints with alternate layers of PA, and PA reinforced with continuous CF [22], aluminium single-lap joints with polyphenylene sulfide (PPS) reinforced with CF [85], and aluminium-carbon fiber reinforced polymer (CFRP) single-lap joints glued with an epoxy adhesive [86] or with an epoxy adhesive with carbon

nanotubes (CNTs) [89]. It is also evident from the figure that the ULSS values of the single-lap joints increase when changed from ABS to PA, and from PA to PA + CF, indicating a better strength for the joints produced with PA and PA + CF, possibly due to a greater affinity of the polyamides with aluminium, and to a higher stiffness of the PA + CF. The single-lap joints made with PA + CF were also the ones that presented smoother surfaces and less shrinkage, features that can mitigate the delamination of the polymers from the aluminium substrate [88]. The values of ULSS for SP and GB aluminium-PA single lap joints were 2.5 and 3.8 MPa, respectively. These values are in line with the ones reported by Boutar et al. [84] for aluminium-aluminium single-lap joints glued with a PU adhesive (2.9 MPa), achieved for the same level of surface roughness of the substrate ( $R_a = 0.30 \mu\text{m}$ ), but below the value of 6.5 MPa reported by Musiari et al. [87], which was obtained with a higher surface roughness of the substrate, with  $R_a = 3.15 \mu\text{m}$ .

The ULSS values of single-lap joints, where the aluminium substrate was subjected to the GB technique, were 1.0, 3.8, and 6.6 MPa for the ABS, PA, and PA + CF adherents, respectively. The ULSS value for the aluminium-ABS single-lap joint is in accordance with that reported by Bechtel et al. [83] ( $\sim 1$  MPa) and by Falck et al. [23] (0.9–1.6 MPa), and below that reported by the same author in [22] (5.3 MPa) obtained for higher values of surface roughness values ( $R_c = 89.0 \pm 0.3 \mu\text{m}$ ) compared to those reported in this work ( $R_c = 6.20 \pm 1.67 \mu\text{m}$ ). For these aluminium-ABS joints, lower ULSS values might be the result of the primer's application process and the nonexistence of a thermal post-processing of the metallic adherend prior to adhesion with the ABS top adherent, since the build plate temperature significantly influences the ULSS value, as demonstrated by Bechtel et al. [83].

The ULSS value for single-lap joints with PA + CF (6.6 MPa) can be compared with the value obtained by Musiari et al. [87] (6.5 MPa) and with that found by Falck et al. [22] for single-lap joints made of aluminium with alternate layers of PA and PA with continuous carbon fibers (21.9 MPa). The discrepancy found in these results may be explained by multiple factors: a larger surface roughness of the substrate (as a vehicle for good adhesion among polymer/metal joints), and the use of continuous carbon fibers that will enhance the stiffness of the joint and increase its ULSS.

### 3.4. Fracture and Failure Modes

An analysis of the fractured surfaces of the joints was undertaken aiming to correlate the adhesion performance of each joint with the resulting failure mode.

The aluminium-PA single lap joints with the substrate abraded by SP, and this showed a fractured surface characterized by poor adhesion between both adherends. An adhesive failure mode is clearly defined, indicating poor wetting of the substrate surface, as shown in Figure 7a. Contrary to this, the aluminium-PA + CF single lap joints with the substrate abraded by SP displays a cohesive failure mode, where the PA + CF coating is strongly adhered to the aluminium substrate, and is shown in Figure 7b. These observations corroborate the previously described mechanical results that indicate that in joints where the substrate was abraded by SP, the PA + CF specimens perform better than the PA type specimens. The better adhesion of aluminium-PA + CF single lap joints can be explained by a positive effect of the presence of fibers in the adhesion between aluminium and PA and by the effect of remelting the primer, enhancing the mechanical interlocking between the aluminium and PA.

The aluminium-ABS single-lap joints with the substrate abraded by GB displays a critical adhesive failure mode between the ABS and the aluminium substrate that is probably due to the poor wetting of its surface, shown in Figure 7c. The same adhesive failure mode on aluminium-ABS single-lap joints, with the substrate abraded by GB, was identified in 3D printed samples [83]. On aluminium-PA single-lap joints with the substrate abraded by GB, the fractured surfaces reveal a mixed adhesive/cohesive failure mode (Figure 7d), while in the aluminium-PA + CF single-lap joints with the substrate abraded by GB, the fracture occurred in the PA + CF region outside the zone of the joint, as shown in Figure 7e. These observations are in agreement with the results from the mechanical

tests, which assign the highest ULSS values to joints made with PA and PA + CF, and can be justified by a good adhesion between aluminium and PA or PA + CF, due to higher values of the surface roughness of aluminium, and due to the remelt of the primer that enabled the flow of the polymer-based materials into the aluminium surface cavities, enhancing the mechanical interlocking between the two materials.

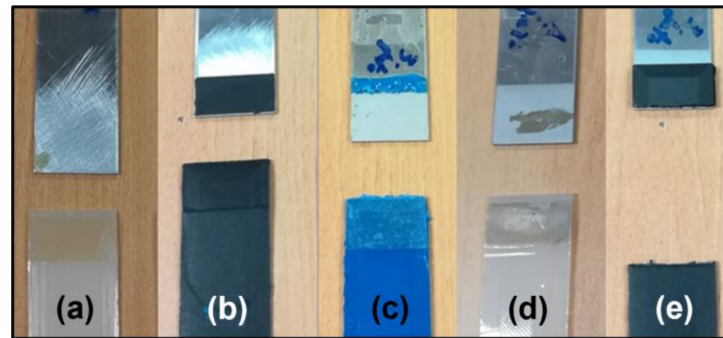


**Figure 7.** Photograph of each single-lap joint's failure mode: (a) aluminium-PA abraded by SP, (b) aluminium-PA + CF abraded by SP, (c) aluminium-ABS abraded by GB, (d) aluminium-PA + CF abraded by GB, and (e) aluminium-PA + CF abraded by GB.

#### 4. Conclusions

In this work, the feasibility of adhesion between aluminium and three polymer-based materials: ABS, PA, and PA + CF, was studied. The effect of the substrate surface roughness and the presence of fibers on the adhesion strength between each pair of materials was determined.

The aluminium's substrate was mechanically abraded by the SP and GB techniques, giving rise to two types of surface roughness values in addition to that of the non-abraded metal, thus  $R_a = 0.16 \mu\text{m}$  for the non-abraded surface,  $R_a = 0.32 \mu\text{m}$  for the surface abraded by SP, and  $R_a = 1.65 \mu\text{m}$  for the surface abraded by GB. Despite the fact that the use of SP for abrasion purposes has been extensively studied for different types of joints, its use in joints manufactured by FFF processes requires further discussion. The GB technique proved to be superior, leading to higher ULSS values.

The following procedures depended on the choice of polymer. For ABS, a solution was manually applied on top of the aluminium substrate, followed by a short curing time before the ABS filament was deposited on top of that. For PA and PA + CF, the application of the primer was done by FFF, which was then remelted on top of a hot plate.

The SEM's analysis of the cross section of the PMHM joints reveals the characteristic layered structure of the 3D printed polymer-based materials, and indicates a thickness of 0.125 mm for the aluminium-ABS single lap joints, validating the programmed 0.1 mm primer's thickness for the PMHM joints produced with PA and PA + CF and, thus, reinforcing the relevance of the FFF technology on the primer fabrication processes.

The mechanical strength of PMHM single-lap joints produced by FFF increases for substrates with a higher surface roughness, the remelting of the primer (PA and PA + CF), and the higher stiffness of the polymer-based adherent.

The mechanical strength of the studied single-lap joints was in good agreement with the reported values in the literature when the same levels of surface roughness of the substrate were considered. The results obtained in this work demonstrate the suitability of filaments with short carbon fibers in producing PMHM joints by FFF. The filaments with short carbon fibers might be a viable alternative for expensive continuous carbon filaments, also allowing their use in a broader range of 3D machines.

The analysis of the fractured surface of the joints allowed for the correlation of the adhesion performance of each joint with the resulting failure mode. Depending on the surface roughness level of the aluminium and the polymer-based material, adhesive, cohesive or substrate failures modes were identified.

Overall, this work validated the FFF technique for a novel combination of materials, aluminium-PA and aluminium-(PA + CF). Aluminium-(PA + CF) single-lap joints exhibited the best mechanical properties, due to the inherent stiffness of the PA + CF and the application of the thermal treatment on the primer. The thermal treatment of the primer proved to be extremely advantageous when looking for a PMH component's fabrication. This is an element that can be easily added to a standard FFF process. Future works might include the introduction of an adhesive fillet by FFF in the end region of the joint and the studying of the aluminium-(PA + CF) single-lap joints, considering higher values for the surface roughness of aluminium.

The advances in this technology could promote the utilization of FFF processes as a complementary manufacturing technique for lightweight components, such as those used in the transportation sector.

**Supplementary Materials:** The following supporting information can be downloaded at: <https://www.mdpi.com/article/10.3390/app13074429/s1>, Figure S1. Aluminium-PA Joints with the aluminium substrate abraded by SP. Figure S2. Aluminium-(PA+CF) Joints with the aluminium substrate abraded by SP. Figure S3. Aluminium-ABS Joints with the aluminium substrate abraded by GB. Figure S4. Aluminium-PA Joints with the aluminium substrate abraded by GB. Figure S5. Aluminium-(PA+CF) Joints with the aluminium substrate abraded by GB.

**Author Contributions:** Conceptualization, C.M.S.V. and M.L.; methodology, G.M., C.M.S.V. and M.L.; formal analysis, G.M.; investigation, G.M.; resources, M.L.; writing—original draft preparation, G.M.; writing—review and editing, C.M.S.V. and M.L.; supervision, C.M.S.V. and M.L. All authors have read and agreed to the published version of the manuscript.

**Funding:** This work was supported by FCT—Fundação para a Ciência e Tecnologia, through IDMEC, under LAETA, Project UIDB/50022/2020. The authors also gratefully acknowledge the funding of the FCT project, AM Optical, PTDC/EME-EME/4593/2021.

**Institutional Review Board Statement:** Not applicable.

**Informed Consent Statement:** Not applicable.

**Data Availability Statement:** Not applicable.

**Conflicts of Interest:** The authors declare that they have no conflict of interest.

## References

1. United Nations General Assembly. *Transforming Our World: The 2030 Agenda for Sustainable Development*; United Nations: New York, NY, USA, 2015.
2. European Commission. *The European Green Deal*; European Commission: Brussels, Belgium, 2019.
3. European Commission. *A New Industrial Strategy for Europe*; European Commission: Brussels, Belgium, 2020.
4. Sankaranarayanan, R.; Hynes, N.R.J. Prospects of Joining Multi-Material Structures. *AIP Conf. Proc.* **2018**, *1953*, 130021. [[CrossRef](#)]
5. Martinsen, K.; Hu, S.J.; Carlson, B.E. Joining of Dissimilar Materials. *CIRP Ann.* **2015**, *64*, 679–699. [[CrossRef](#)]
6. Haghshenas, M.; Gerlich, A.P. Joining of Automotive Sheet Materials by Friction-Based Welding Methods: A Review. *Eng. Sci. Technol. Int. J.* **2018**, *21*, 130–148. [[CrossRef](#)]
7. Taghipoor, H.; Eyvazian, A. Quasi-Static Axial Crush Response and Energy Absorption of Composite Wrapped Metallic Thin-Walled Tube. *J. Braz. Soc. Mech. Sci. Eng.* **2022**, *44*, 158. [[CrossRef](#)]
8. Elmi Hosseini, S.R.; Fernandes, F.A.O.; Pereira, A.B.; Li, Z. *Welding of Dissimilar Materials in Aerospace Systems*; Springer Nature: Cham, Switzerland, 2022; pp. 317–344. [[CrossRef](#)]
9. Chen, H.-C.; Pinkerton, A.J.; Li, L. Fibre Laser Welding of Dissimilar Alloys of Ti-6Al-4V and Inconel 718 for Aerospace Applications. *Int. J. Adv. Manuf. Technol.* **2011**, *52*, 977–987. [[CrossRef](#)]
10. Taghipoor, H.; Sefidi, M. Energy Absorption of Foam-Filled Corrugated Core Sandwich Panels under Quasi-Static Loading. *Proc. Inst. Mech. Eng. Part L J. Mater. Des. Appl.* **2023**, *237*, 234–246. [[CrossRef](#)]
11. Shim, H.; McCullough, E.A.; Jones, B.W. Using Phase Change Materials in Clothing. *Text. Res. J.* **2001**, *71*, 495–502. [[CrossRef](#)]
12. Levy, G.N.; Schindel, R.; Kruth, J.P. Rapid Manufacturing and Rapid Tooling with Layer Manufacturing (LM) Technologies, State of the Art and Future Perspectives. *CIRP Ann.* **2003**, *52*, 589–609. [[CrossRef](#)]
13. Bahraminasab, M.; Sahari, B.B.; Edwards, K.L.; Farahmand, F.; Hong, T.S.; Arumugam, M.; Jahan, A. Multi-Objective Design Optimization of Functionally Graded Material for the Femoral Component of a Total Knee Replacement. *Mater. Des.* **2014**, *53*, 159–173. [[CrossRef](#)]

14. MacDonald, E.; Wicker, R. Multiprocess 3D Printing for Increasing Component Functionality. *Science* **2016**, *353*, aaf2093. [[CrossRef](#)]
15. Berman, B. 3-D Printing: The New Industrial Revolution. *Bus. Horiz.* **2012**, *55*, 155–162. [[CrossRef](#)]
16. Dumitrescu, G.C.; Tanase, I.A. 3D Printing—A New Industrial Revolution. *Knowl. Horizons Econ.* **2016**, *8*, 32–39.
17. Kah, P.; Suoranta, R. Techniques for Joining Dissimilar Materials: Metals and Polymers. *Rev. Adv. Mater. Sci.* **2014**, *36*, 152–164.
18. Gonzales, D.S.; Alvarez, A.G. *Additive Manufacturing Feasibility Study and Technology Demonstration EDA AM—State of the Art and Strategic Report*; European Defence Agency: Ixelles, Belgium, 2018; pp. 1–187.
19. Vaezi, M.; Chianrabutra, S.; Mellor, B.; Yang, S. Multiple Material Additive Manufacturing—Part 1: A Review. *Virtual Phys. Prototyp.* **2013**, *8*, 19–50. [[CrossRef](#)]
20. *ISO/ASTM 52900:2021; Additive Manufacturing—General Principles—Fundamentals and Vocabulary*. ISO: Geneva, Switzerland, 2021. [[CrossRef](#)]
21. Fafenrot, S.; Grimmelsmann, N.; Wortmann, M.; Ehrmann, A. Three-Dimensional (3D) Printing of Polymer-Metal Hybrid Materials by Fused Deposition Modeling. *Materials* **2017**, *10*, 1199. [[CrossRef](#)]
22. Falck, R.; Goushegir, S.M.; dos Santos, J.F.; Amancio-Filho, S.T. AddJoining: A Novel Additive Manufacturing Approach for Layered Metal-Polymer Hybrid Structures. *Mater. Lett.* **2018**, *217*, 211–214. [[CrossRef](#)]
23. Falck, R.; dos Santos, J.F.; Amancio-Filho, S.T. Microstructure and Mechanical Performance of Additively Manufactured Aluminium 2024-T3/Acrylonitrile Butadiene Styrene Hybrid Joints Using an AddJoining Technique. *Materials* **2019**, *12*, 864. [[CrossRef](#)]
24. Turner, B.N.; Strong, R.; Gold, S.A. A Review of Melt Extrusion Additive Manufacturing Processes: I. Process Design and Modeling. *Rapid Prototyp. J.* **2014**, *20*, 192–204. [[CrossRef](#)]
25. Shrivastava, A. Introduction to Plastics Engineering. In *Introduction to Plastics Engineering*; Elsevier: Cambridge, MA, USA, 2018; pp. 1–16. [[CrossRef](#)]
26. Langford, W. *Achieving Precise Flow in Fused Deposition Modeling Extruders*; Term Paper—Engineering Management; Tufts University: Medford, MA, USA, 2012.
27. Turner, B.N.; Gold, S.A. A Review of Melt Extrusion Additive Manufacturing Processes: II. Materials, Dimensional Accuracy, and Surface Roughness. *Rapid Prototyp. J.* **2015**, *21*, 250–261. [[CrossRef](#)]
28. Lalegani Dezaki, M.; Mohd Ariffin, M.K.A.; Hatami, S. An Overview of Fused Deposition Modelling (FDM): Research, Development and Process Optimisation. *Rapid Prototyp. J.* **2021**, *27*, 562–582. [[CrossRef](#)]
29. Anitha, R.; Arunachalam, S.; Radhakrishnan, P. Critical Parameters Influencing the Quality of Prototypes in Fused Deposition Modelling. *J. Mater. Process. Technol.* **2001**, *118*, 385–388. [[CrossRef](#)]
30. Van Weeren, R.; Agarwala, M.; Jamalabad, V.R.; Bandyopadhyay, A.; Vaidyanathan, R.; Langrana, N.; Safari, A.; Whalen, P.; Danforth, S.C.; Ballard, C. Quality of Parts Processed by Fused Deposition. In *Proceedings of the International Solid Freeform Fabrication Symposium*, Austin, TX, USA, 7–9 August 1995. [[CrossRef](#)]
31. Agarwala, M.K.; Jamalabad, V.R.; Langrana, N.A.; Safari, A.; Whalen, P.J.; Danforth, S.C. Structural Quality of Parts Processed by Fused Deposition. *Rapid Prototyp. J.* **1996**, *2*, 4–19. [[CrossRef](#)]
32. Dey, A.; Yodo, N. A Systematic Survey of FDM Process Parameter Optimization and Their Influence on Part Characteristics. *J. Manuf. Mater. Process.* **2019**, *3*, 64. [[CrossRef](#)]
33. Sood, A.K.; Ohdar, R.K.; Mahapatra, S.S. Improving Dimensional Accuracy of Fused Deposition Modelling Processed Part Using Grey Taguchi Method. *Mater. Des.* **2009**, *30*, 4243–4252. [[CrossRef](#)]
34. Kuznetsov, V.E.; Solonin, A.N.; Urzhumtsev, O.D.; Schilling, R.; Tavitov, A.G. Strength of PLA Components Fabricated with Fused Deposition Technology Using a Desktop 3D Printer as a Function of Geometrical Parameters of the Process. *Polymer* **2018**, *10*, 313. [[CrossRef](#)]
35. Sun, Q.; Rizvi, G.M.; Bellehumeur, C.T.; Gu, P. Effect of Processing Conditions on the Bonding Quality of FDM Polymer Filaments. *Rapid Prototyp. J.* **2008**, *14*, 72–80. [[CrossRef](#)]
36. Vicente, C.M.S.; Martins, T.S.; Leite, M.; Ribeiro, A.; Reis, L. Influence of Fused Deposition Modeling Parameters on the Mechanical Properties of ABS Parts. *Polym. Adv. Technol.* **2020**, *31*, 501–507. [[CrossRef](#)]
37. Bagsik, A.; Schöppner, V. Mechanical Properties of Fused Deposition Modeling Parts Manufactured with ULTEM 9085. In *Proceedings of the 69th Annual Technical Conference of the Society of Plastics Engineers (ANTEC'11)*, Boston, MA, USA, 1–5 May 2011.
38. Magnus, C. Feasibility Study of Metal to Polymer Hybrid Joinin. Master's Thesis, Lappeenranta University of Technology, Lappeenranta, Finland, 2012.
39. Troschitz, J.; Vorderbrüggen, J.; Kupfer, R.; Gude, M.; Meschut, G. Joining of Thermoplastic Composites with Metals Using Resistance Element Welding. *Appl. Sci.* **2020**, *10*, 7251. [[CrossRef](#)]
40. Popp, J.; Römisch, D.; Merklein, M.; Drummer, D. Joining of CFRT/Steel Hybrid Parts via Direct Pressing of Cold Formed Non-Rotational Symmetric Pin Structures. *Appl. Sci.* **2022**, *12*, 4962. [[CrossRef](#)]
41. Petrie, E.M. Adhesive Bonding of Textiles: Principles, Types of Adhesive and Methods of Use. In *Joining Textiles Principles and Applications*; Elsevier: Cambridge, MA, USA, 2013; pp. 225–274. [[CrossRef](#)]
42. Chawla, K.K. *Composite Materials*; Springer: New York, NY, USA, 2012; ISBN 978-0-387-74364-6.
43. Ebnesajjad, S. Material Surface Preparation Techniques. In *Handbook of Adhesives and Surface Preparation Technology, Applications and Manufacturing*; Elsevier: Cambridge, MA, USA, 2011; pp. 49–81. [[CrossRef](#)]
44. Derjaguin, B.V.; Smilga, V.P. Electronic Theory of Adhesion. *J. Appl. Phys.* **2004**, *38*, 4609. [[CrossRef](#)]

45. Possart, W. Experimental and Theoretical Description of the Electrostatic Component of Adhesion at Polymer/Metal Contacts. *Int. J. Adhes. Adhes.* **1988**, *8*, 77–83. [CrossRef]
46. Awaja, F.; Gilbert, M.; Kelly, G.; Fox, B.; Pigram, P.J. Adhesion of Polymers. *Prog. Polym. Sci.* **2009**, *34*, 948–968. [CrossRef]
47. Baldan, A. Adhesion Phenomena in Bonded Joints. *Int. J. Adhes. Adhes.* **2012**, *38*, 95–116. [CrossRef]
48. Wang, H. Improving the Adhesion of Polyethylene by UV Grafting. *J. Adhes.* **2006**, *82*, 731–745. [CrossRef]
49. Tang, H.; Martin, D.C. Microstructural Studies of Interfacial Deformation in Painted Thermoplastic Polyolefins (TPOs). *J. Mater. Sci.* **2002**, *37*, 4783–4791. [CrossRef]
50. Voyutskii, S.S.; Vakula, V.L. The Role of Diffusion Phenomena in Polymer-to-Polymer Adhesion. *J. Appl. Polym. Sci.* **1963**, *7*, 475–491. [CrossRef]
51. Bikerman, J.J. Causes of Poor Adhesion: Weak Boundary Layers. *Ind. Eng. Chem.* **2002**, *59*, 40–44. [CrossRef]
52. Nenakhov, S.A. Basic Terms and Definitions in Adhesion. *Polym. Sci. Ser. D* **2008**, *1*, 19–22. [CrossRef]
53. Li, J.; Xia, L.; Li, P.; Zhu, Y.; Sun, Y.; Zuo, D. Relationship between Coefficient of Friction and Surface Roughness of Wafer in Nanomachining Process. *SPIE* **2013**, *8793*, 87931Y. [CrossRef]
54. Ochoa-Putman, C.; Vaidya, U.K. Mechanisms of Interfacial Adhesion in Metal–Polymer Composites—Effect of Chemical Treatment. *Compos. A Appl. Sci. Manuf.* **2011**, *42*, 906–915. [CrossRef]
55. Chueh, Y.H.; Wei, C.; Zhang, X.; Li, L. Integrated Laser-Based Powder Bed Fusion and Fused Filament Fabrication for Three-Dimensional Printing of Hybrid Metal/Polymer Objects. *Addit. Manuf.* **2020**, *31*, 100928. [CrossRef]
56. Islam, M.S.; Tong, L.; Falzon, P.J. Influence of Metal Surface Preparation on Its Surface Profile, Contact Angle, Surface Energy and Adhesion with Glass Fibre Prepreg. *Int. J. Adhes. Adhes.* **2014**, *51*, 32–41. [CrossRef]
57. Harris, A.F.; Beevers, A. The Effects of Grit-Blasting on Surface Properties for Adhesion. *Int. J. Adhes. Adhes.* **1999**, *19*, 445–452. [CrossRef]
58. Petrie, E.M. *Handbook of Adhesives and Sealants*; McGraw-Hill Education: New York, NY, USA, 2007.
59. Objois, A.; Gilibert, Y.; Fargette, B. Theoretical and Experimental Analysis of the Scarf Joint Bonded Structure: Influence of the Adhesive Thickness on the Micro-Mechanical Behavior. *J. Adhes.* **1999**, *70*, 13–32. [CrossRef]
60. Duncan, B.C.; Crocker, L.E. *Review of Tests for Adhesion Strength*; National Physical Laboratory: Middlesex, UK, 2001.
61. Yilmaz, B.; Asokkumar, A.; Jasiūnienė, E.; Kažys, R.J. Air-Coupled, Contact, and Immersion Ultrasonic Non-Destructive Testing: Comparison for Bonding Quality Evaluation. *Appl. Sci.* **2020**, *10*, 6757. [CrossRef]
62. Barile, C.; Casavola, C.; Pappalettera, G.; Vimalathithan, P.K. Multiparameter Approach for Damage Propagation Analysis in Fiber-Reinforced Polymer Composites. *Appl. Sci.* **2021**, *11*, 393. [CrossRef]
63. Olivera, S.; Muralidhara, H.B.; Venkatesh, K.; Gopalakrishna, K.; Vivek, C.S. Plating on Acrylonitrile–Butadiene–Styrene (ABS) Plastic: A Review. *J. Mater. Sci.* **2016**, *51*, 3657–3674. [CrossRef]
64. Arnold, J. High Quality Copper-Nickel-Chromium Plating on Plastics: A Continuous Process and Its Challenges. *Plat. Surf. Finish.* **2004**, *91*, 38–47.
65. Zhang, H.; Shen, L.; Chang, J. Comparative Study of Electroless Ni-p, Cu, Ag, and Cu-Ag Plating on Polyamide Fabrics. *J. Ind. Text.* **2011**, *41*, 25–40. [CrossRef]
66. Giraud, D.; Borit, F.; Guipont, V.; Jeandin, M.; Malhaire, J.M. Metallization of a Polymer Using Cold Spray: Application to Aluminum Coating of Polyamide 66. In Proceedings of the International Thermal Spray Conference, Houston, TX, USA, 21–24 May 2012; pp. 265–270. [CrossRef]
67. Dielectric Manufacturing ABS Material Properties. Available online: <https://dielectricmfg.com/knowledge-base/abs/> (accessed on 15 December 2022).
68. Cantrell, J.; Rohde, S.; Damiani, D.; Gurnani, R.; DiSandro, L.; Anton, J.; Young, A.; Jerez, A.; Steinbach, D.; Kroese, C.; et al. Experimental Characterization of the Mechanical Properties of 3D Printed ABS and Polycarbonate Parts. In *Conference Proceedings of the Society for Experimental Mechanics Series*; Springer: New York, NY, USA, 2017; Volume 3, pp. 89–105. ISBN 9783319415994.
69. Dawoud, M.; Taha, I.; Ebeid, S.J. Mechanical Behaviour of ABS: An Experimental Study Using FDM and Injection Moulding Techniques. *J. Manuf. Process.* **2016**, *21*, 39–45. [CrossRef]
70. Novakova-Marcincinova, L.; Novak-Marcincin, J. Testing of Materials for Rapid Prototyping Fused Deposition Modelling Technology. *Int. J. Ind. Manuf. Eng.* **2012**, *6*, 2082–2085. [CrossRef]
71. Gilbert, M. *Aliphatic Polyamides*. *Brydson's Plastics Materials*, 8th ed.; Butterworth-Heinemann: Oxford, UK, 2017; pp. 487–511. [CrossRef]
72. Sardinha, M.; Vicente, C.M.S.; Frutuoso, N.; Leite, M.; Ribeiro, R.; Reis, L. Effect of the Ironing Process on ABS Parts Produced by FDM. *Mater. Des. Process. Commun.* **2021**, *3*, e151. [CrossRef]
73. Wang, T.M.; Xi, J.T.; Jin, Y. A Model Research for Prototype Warp Deformation in the FDM Process. *Int. J. Adv. Manuf. Technol.* **2006**, *33*, 1087–1096. [CrossRef]
74. Cham, J.G.; Pruitt, B.L.; Cutkosky, M.R.; Binnard, M.; Weiss, L.E.; Neplotnik, G. Layered Manufacturing with Embedded Components: Process Planning Considerations. *Proc. ASME Des. Eng. Tech. Conf.* **1999**, *4*, 93–101. [CrossRef]
75. Mieszala, M.; Hasegawa, M.; Guillonneau, G.; Bauer, J.; Raghavan, R.; Frantz, C.; Kraft, O.; Mischler, S.; Michler, J.; Philippe, L. Micromechanics of Amorphous Metal/Polymer Hybrid Structures with 3D Cellular Architectures: Size Effects, Buckling Behavior, and Energy Absorption Capability. *Small* **2017**, *13*, 1602514. [CrossRef]

76. ASTM Standard Test Method for Determining Strength of Adhesively Bonded Rigid Plastic Lap-Shear Joints in Shear by Tension Loading. Available online: <https://www.astm.org/d3163-01r14.html> (accessed on 14 December 2022).
77. *ASTM Standard E8/E8M-13a*; Standard Test Methods for Tension Testing of Metallic Materials. ASTM International: West Conshohocken, PA, USA, 2013; pp. 1–27.
78. Markforged Material Datasheet Composites. Available online: <https://static.markforged.com/downloads/composites-data-sheet.pdf> (accessed on 15 December 2022).
79. Fillamentum 3D Printing Guide—Fillamentum Nylon CF15 Carbon. Available online: [http://www.fillamentumautomotive.com/wp-content/uploads/2020/10/FI\\_Printing\\_Guide\\_Nylon\\_CF15\\_Carbon.pdf](http://www.fillamentumautomotive.com/wp-content/uploads/2020/10/FI_Printing_Guide_Nylon_CF15_Carbon.pdf) (accessed on 15 December 2022).
80. Spoerk, M.; Gonzalez-Gutierrez, J.; Sapkota, J.; Schuschnigg, S.; Holzer, C. Effect of the Printing Bed Temperature on the Adhesion of Parts Produced by Fused Filament Fabrication. *Plast. Rubber Compos.* **2018**, *47*, 17–24. [CrossRef]
81. Ghumatkar, A.; Budhe, S.; Sekhar, R.; Banea, M.D.; De Barros, S. Influence of Adherend Surface Roughness on the Adhesive Bond Strength. *Lat. Am. J. Solids Struct.* **2016**, *13*, 2356–2370. [CrossRef]
82. Filmetrics ProfilomOnline—Surface Imaging, Analysis, and Measurement Software for 3D Profilometers and AFMs. Available online: <https://www.profilmonline.com/> (accessed on 27 December 2022).
83. Bechtel, S.; Schweitzer, R.; Frey, M.; Busch, R.; Herrmann, H.-G. Material Extrusion of Structural Polymer–Aluminum Joints—Examining Shear Strength, Wetting, Polymer Melt Rheology and Aging. *Materials* **2022**, *15*, 3120. [CrossRef]
84. Boutar, Y.; Naïmi, S.; Mezlini, S.; Ali, M.B.S. Effect of Surface Treatment on the Shear Strength of Aluminium Adhesive Single-Lap Joints for Automotive Applications. *Int. J. Adhes. Adhes.* **2016**, *67*, 38–43. [CrossRef]
85. Goushegir, S.M.; dos Santos, J.F.; Amancio-Filho, S.T. Influence of Aluminum Surface Pre-Treatments on the Bonding Mechanisms and Mechanical Performance of Metal-Composite Single-Lap Joints. *Weld. World* **2017**, *61*, 1099–1115. [CrossRef]
86. Darla, V.; Satish Ben, B.; Sai Srinadh, K.; Venkata Rao, K. Evaluation of Aluminum to Composite Bonded Lap Joints. *High Perform. Polym.* **2022**, *34*, 1152–1163. [CrossRef]
87. Musiari, F.; Moroni, F. Experimental Study of the Influence of the Surface Preparation on the Fatigue Behavior of Polyamide Single Lap Joints. *Materials* **2021**, *14*, 1008. [CrossRef] [PubMed]
88. Lucchetta, G.; Marinello, F.; Bariani, P.F. Aluminum Sheet Surface Roughness Correlation with Adhesion in Polymer Metal Hybrid Overmolding. *CIRP Ann.* **2011**, *60*, 559–562. [CrossRef]
89. Cheng, F.; Hu, Y.; Zhang, X.; Hu, X.; Huang, Z. Adhesive Bond Strength Enhancing between Carbon Fiber Reinforced Polymer and Aluminum Substrates with Different Surface Morphologies Created by Three Sulfuric Acid Solutions. *Compos. A Appl. Sci. Manuf.* **2021**, *146*, 106427. [CrossRef]

**Disclaimer/Publisher’s Note:** The statements, opinions and data contained in all publications are solely those of the individual author(s) and contributor(s) and not of MDPI and/or the editor(s). MDPI and/or the editor(s) disclaim responsibility for any injury to people or property resulting from any ideas, methods, instructions or products referred to in the content.